Desalination and Water Treatment
www.deswater.com

doi: 10.5004/dwt.2018.22059

119 (2018) 150–159
July

Study of energy recovery efficiency in a sliding vane pressure exchanger for a SWRO system

Fanghua Ye, Jianqiang Deng*, Zheng Cao, Kai Liu

School of Chemical Engineering and Technology, Xi'an Jiaotong University, Xi'an 710049, China, Tel./Fax: +86 29 82663413; emails: dengjq@mail.xjtu.edu.cn (J. Deng), jkzx4416176@stu.xjtu.edu.cn (F. Ye), czczkok@stu.xjtu.edu.cn (Z. Cao), liukaibk@stu.xjtu.edu.cn (K. Liu)

Received 7 August 2017; Accepted 18 December 2017

ABSTRACT

Sliding vane pressure exchanger (SVPE) is expected to be a type of efficient device to recover pressure energy from liquid streams in seawater reverse osmosis system. In this work, a matching design of vane number and port position was proposed to eliminate the short circuit flow, reversed flow, liquid decompression and compression. The contact performance between the cylinder and vane was studied by the proposed vane dynamic model. Then, the vane dynamics model in conjunction with the energy loss model was used to evaluate the energy recovery efficiency of the SVPE. The critical condition of the contact performance and the energy recovery efficiency of the SVPE were simulated by using MATLAB software. The simulated results in this work were compared with those in the reference. Finally, the influences of the device parameters on the energy recovery efficiency of the SVPE were discussed. According to the simulated results, a careful selection of the device parameters, such as rotational speed, vane thickness and vane length, is critical in order to improve the energy recovery efficiency of the SVPE. This work may provide a vital method to accurately predict the energy recovery efficiency of the SVPE, and help to guide the performance optimization.

Keywords: Desalination; Energy recovery efficiency; Sliding vane pressure exchanger; Seawater reverse osmosis system

1. Introduction

Over the years, the efficient use of energy sources has shifted people's much concern. As is known to all, the most common energy forms that can be recovered are heat and pressure. According to the developed heat exchange technology, the heat energy recovery potential is distributed in numerous processes with temperature difference. Analogously, the pressure energy recovery can be accomplished by pressure energy exchange between process streams with pressure difference. These streams exit in most pressure-driven process industries, such as membrane industry, chemical industry, food industry and seawater desalination industry.

Seawater reverse osmosis (SWRO) technology has been proved as a significantly efficient way in seawater desalination to deal with the shortage of fresh water [1]. Nevertheless, there are still a lot of restraints that blocks the development of the SWRO technology, especially the high energy consumption. Numerous efforts have been done in order to decrease the energy consumption in the SWRO system, such as the configuration optimization of reverse osmosis (RO) arrays [2], the improvement of the hydraulic permeability of RO membranes [3] and the application of energy recovery devices (ERDs) [4]. It has been proved that the application of ERDs in the SWRO system can obviously decrease the energy consumption [5] and make the production of fresh water economical with low carbon emission.

Several kinds of ERDs have been developed to recover the remaining pressure energy [6]. Presently, ERDs based on the positive displacement principle mainly include the piston-type work exchanger and the rotary pressure exchanger [7]. Due to the distinct advantage of high energy

* Corresponding author.

Presented at 2017 Qingdao International Water Congress, June 27–30, 2017, Qingdao, China.

recovery efficiency of about 96.6% [8], the PX pressure exchanger produced by Energy Recovery, Inc., as a typical commercial product of the rotary pressure exchanger, has been a critical component to decrease the energy consumption in the SWRO system [9]. It is investigated that over 80% of the newly built SWRO plants are supplied with rotary pressure exchangers [10]. But meanwhile, the rotary pressure exchanger is of difficult manufacture, and the uncontrollable fluid mixing occurs within the device due to the direct contact between brine stream and seawater stream [11]. The piston-type work exchanger is of low fluid mixing rate and high energy recovery efficiency above 90%. But its initial investment cost and maintenance cost are relatively high. Meanwhile, globe valves and servo valves are needed to precisely control the flow directions of fluid streams [12]. In contrast to the positive displacement type ERDs, the centrifugal type ERDs, including Pelton wheels, reverse-running pumps and turbochargers, have a maximum efficiency of about 82% [13].

In recent years, the sliding vane pressure exchanger (SVPE) has been proposed as an ERD [14]. The schematic of SVPE is shown in Fig. 1. It consists of a cylinder, a rotor and several sliding vanes. The sliding vanes fit in the vane slots which are arranged in the rotor. The high pressure brine stream pushes the vane to drive the rotor to rotate at the brine side and entrains the low pressure seawater at the seawater side. The low pressure seawater is pressurized by the vane and flows into high pressure pipe network. The energy is transferred by the rotor and vanes from brine stream to seawater stream.

As shown in Fig. 2, the SWRO system coupled with a SVPE device consists of a seawater supply pump, a high pressure pump, a booster pump, membrane modules and a SVPE device. The brine stream discharged from membrane modules goes through the SVPE device, where its pressure is transferred to a part of (about 60%) seawater stream. A booster pump is arranged downstream the pressurized seawater stream in order to supply the pressure loss in the membrane modules, the SVPE device and the pipeline. Fully pressurized seawater stream then combines with the seawater pumped by the high pressure pump to the SWRO system. And the depressurized brine stream flows out of the SWRO system.

It is a pity that no more literature about the SVPE has been reported so far. In a study by Al-Hawaj [14], models for flow rate, friction loss, leakage loss and efficiency of the device were presented under the assumption that each vane always contacts with the cylinder. The reliable contact between the cylinder and vane is a requirement for the normal operation of the SVPE. However, the assumption of well contact performance has not been validated. Furthermore, an accurate method for precisely predicting the energy recovery efficiency is still necessary to provide detailed characteristics of the SVPE. In this paper, the matching design of the vane number and port position was theoretically proposed. The vane dynamic model was newly established on the basis of the force analysis of the vane. Then, a method was introduced to determine the energy recovery efficiency of the SVPE based on the vane dynamics model and energy loss model. Finally, the influence factors of the energy recovery efficiency and its effects were discussed.

2. Method to determine energy recovery efficiency

2.1. Structural model

As shown in Fig. 1, the rotor is concentrically disposed within the elliptical cylinder inner wall. The rotor turns in the counterclockwise direction. Fig. 3 displays the position of the inlet port and outlet port. The four ports are symmetrically arranged in the cylinder with the port lower edge angular limit of α and the port upper edge angular limit of β. The cylinder profile at the brine side is symmetrical with that at the seawater side, which is divided into five sections by the port edge angles α and β. The five sections are seal section 1, inlet section, middle section, outlet section and seal section 2. And the inlet section and outlet section connect to the inlet port and outlet port, respectively.

Fig. 4 displays the schematic diagram of short circuit flow, reversed flow and liquid decompression and compression in the SVPE. The short circuit flow occurs if there are no vanes located in the middle section at the brine side, as shown in Fig. 4(a). Similarly, at the seawater side, the low

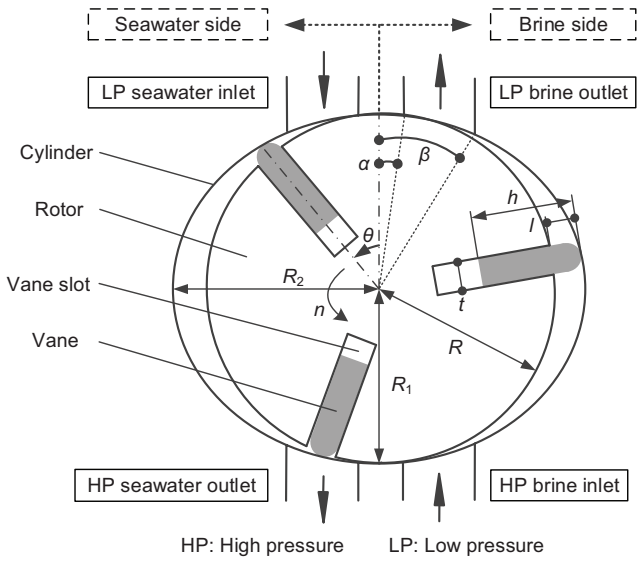

Fig. 1. Schematic of SVPE.

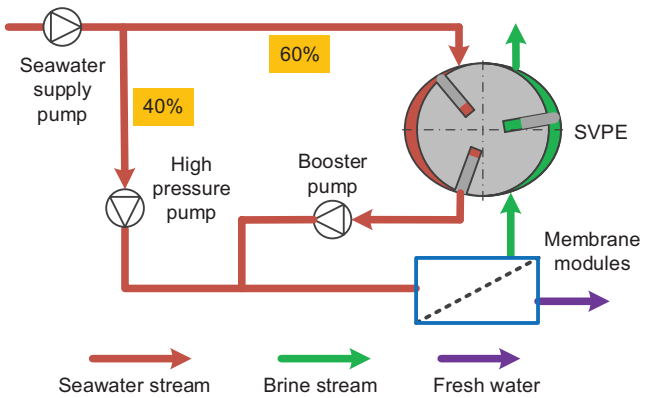

Fig. 2. SWRO system coupled with a SVPE device.

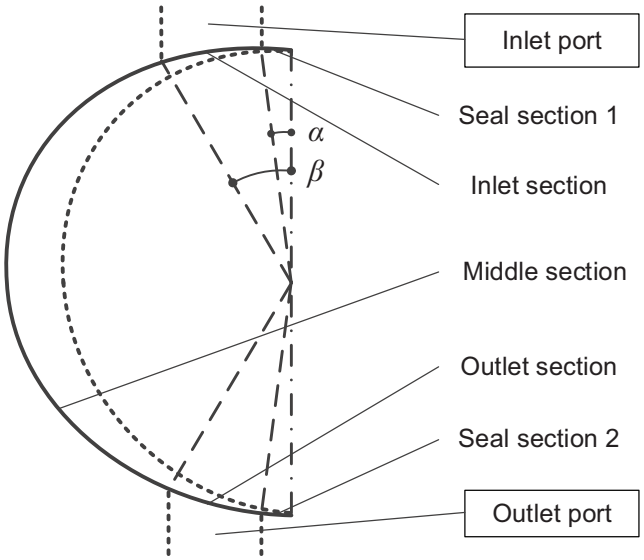

Fig. 3. Positions of inlet port and outlet port.

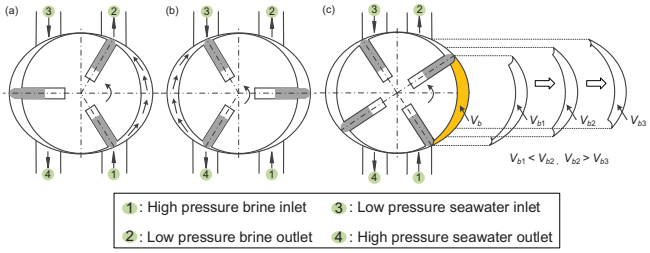

Fig. 4. Schematic diagram of (a) short circuit flow, (b) reversed flow and (c) liquid decompression and compression.

pressure seawater inlet is exposed to the high pressure seawater outlet if there are no vanes located in the middle section, leading to the reversed flow due to the high pressure differential, as shown in Fig. 4(b). Although check valves can be arranged downstream of the seawater inlet to prevent the reversed flow, it will add the complexity of the device and the flow resistance loss of the fluid. In addition, if there are more than one vane located in the middle section, the volume between the two adjacent vanes V_b increases and then decreases when the vane sweeps through the middle section, as shown in Fig. 4(c), leading to the energy loss in the liquid decompression process and the possible damage of the device in the liquid compression process. So, only one vane should be always located in the middle section.

Based on the analysis above, the vane number matched with the port position is proposed in this paper to eliminate the short circuit flow, reversed flow, liquid decompression and compression, and a case of the matching design is presented in Table 1.

2.2. Vane dynamics model

The vane dynamics model takes the following assumptions: (1) the rotational speed of the SVPE is constant. (2) The contact forces act along the vane surface uniformly in the axial direction. (3) The contact point between the cylinder and vane is always located in the top of the vane tip. (4) The manifolds pressure loss is ignored. Several channels are arranged along the front side (downstream side) surface of the vane. The arrangement of the channels provides a flow passage connecting the vane slot bottom and front chamber. The liquid can timely flow into vane slot bottom avoiding the occurrence of low pressure in slot bottom when the vane moves against the rotor center, and the liquid can also timely flow out of vane slot bottom when the vane moves into the rotor center avoiding the occurrence of over pressure in slot bottom. The liquid pressure in the vane bottom can be considered to be the average value of the liquid pressure between in the front chamber and in the rear chamber with a suitable size of the channel [15].

Table 1
A case of the matching design of vane number and port position

Parameter	Value
Number of vanes (z)	3
Lower edge angular limit of port (α)°	5
Upper edge angular limit of port (β)°	30

The vane may not be able to always contact with the cylinder wall. Hence, the forces acting on a single vane whether the vane contacts with the cylinder or not ought to be considered separately, as displayed in Figs. 5(a) and (b). In the two cases, the vane bears the gravitational force F_g, the inertial centrifugal force F_r, the inertial force of convected motion F_e, the Coriolis inertial force F_k, the vane base force F_b acting on the slot bottom due to the liquid pressure in vane slot, the liquid force F_p acting on the vane side due to the liquid pressure difference between two sides of vane, the contact forces F_{n1} and F_{n2} at the two sides of the vane, the friction forces F_{f1} and F_{f2} at the two sides of the vane. In the contact case shown in Fig. 5(a), the liquid forces in the vane tip are divided into two parts, F_{pt1} and F_{pt2}, by the contact point. Also, the contact force F_{nt} and friction force F_{ft} are exerted on the vane tip by the cylinder. In the non-contact case shown in Fig. 5(b), the vane just bears the liquid force F_{pt} in the vane tip. The inertia forces, F_e, F_r and F_k, are associated with vane kinematics. The forces, F_p, F_b, F_{pt}, F_{pt1} and F_{pt2}, are related to the pressure of liquid at two sides of the vane and in the slot bottom at the given angular position. The friction forces, F_{f1}, F_{f2} and F_{ft}, are determined by the Coulomb's friction law. The independent contact forces, F_{n1}, F_{n2} and F_{nt}, can be obtained by solving the force equilibrium equation.

In the contact case shown in Fig. 5(a), the contact forces are calculated by the following matrix equation:

$$KX = F \tag{1}$$

where K, X and F are given as follows:

$$K = \begin{bmatrix} -\cos\delta - \mu_1 \sin\delta & -\mu_2 & -\mu_2 \\ \sin\delta - \mu_1 \cos\delta & 1 & -1 \\ (\sin\delta - \mu_1 \cos\delta)h/2 & -h/2 - \mu_2 t/2 & -(h/2 - h_o) + \mu_2 t/2 \end{bmatrix}$$

$$X = \begin{bmatrix} F_{nt} & F_{n1} & F_{n2} \end{bmatrix}^T$$

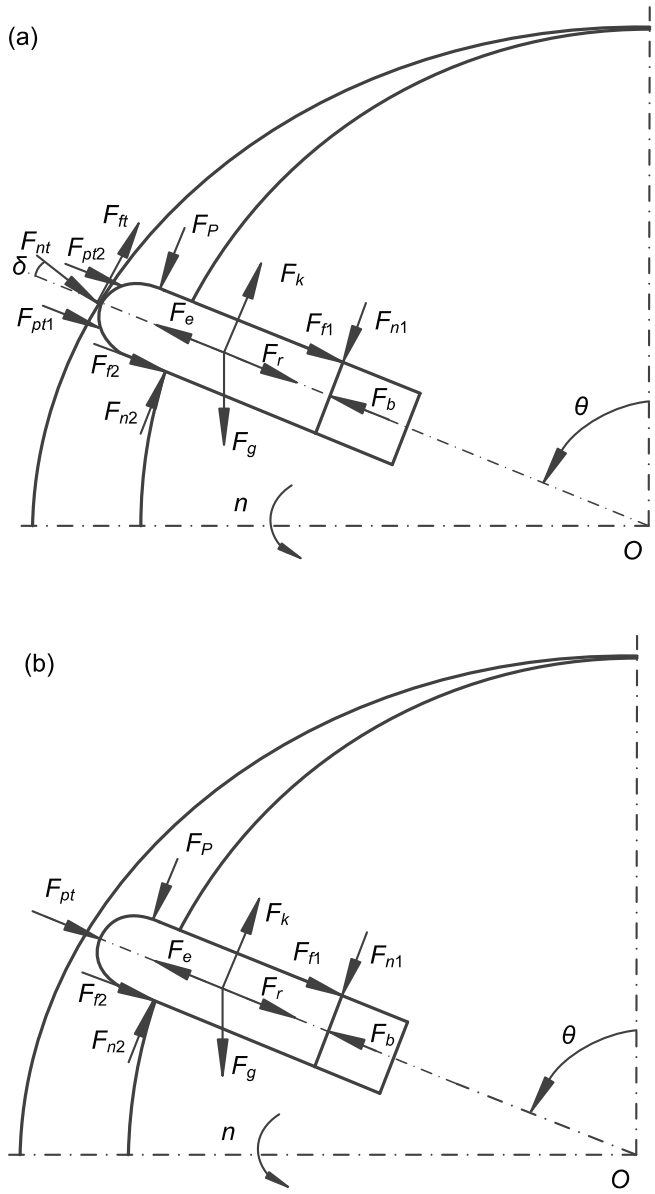

Fig. 5. Forces acting on vane in (a) contact case and (b) non-contact case between cylinder and vane.

$$F = \begin{bmatrix} -F_e + F_r + F_g \sin\theta - F_b + F_{\mathrm{pt1}} + F_{\mathrm{pt2}} \\ F_k + F_g \cos\theta - F_p \\ -F_p(h - h_o)/2 \end{bmatrix}$$

where t is vane thickness, h is vane length in the radial direction, h_o is the length of the vane that extends out of the vane slot, θ is angular position, δ is the inclined angle between vane axis and the normal line at the contact point in the cylinder wall, μ_1 is vane tip friction coefficient, μ_2 is vane side friction coefficient.

In the non-contact case shown in Fig. 5(b), the contact force F_{nt} in the vane tip equals zero, and the vane side contact forces, F_{n1} and F_{n2}, can be obtained by:

$$F_{n1} = \frac{\left(-F_e + F_r + F_g \sin\theta - F_b + F_{\mathrm{pt}}\right)t/2 + \left(F_k + F_g \cos\theta\right)\left(-h/2 + h_o\right) - F_p h_o/2}{-h + h_o - \mu_2 t} \quad (2)$$

$$F_{n2} = F_{n1} - F_k - F_g \cos\theta + F_p \quad (3)$$

It should be noted that the direction of some forces need to be adjusted according to whether the vane extends out of or moves back into the slot, especially the direction of frictional forces F_{f1} and F_{f2}. The dynamic calculation is performed using the force equilibrium equation (Eq. (1)), and then is verified by the contact force F_{nt} of the calculation results. The dynamic calculation is valid if the contact force F_{nt} is positive. Otherwise, the non-contact force equilibrium equations (Eqs. (2) and (3)) instead of Eq. (1) should be used to carry out the dynamic calculation.

2.3. Energy loss model

Defining the energy recovery efficiency of the SVPE as the ratio of the increase in the seawater hydraulic energy to the decrease in the brine hydraulic energy:

$$\eta = \frac{(p_{\mathrm{so}} - p_{\mathrm{si}})q_s}{(p_{\mathrm{bi}} - p_{\mathrm{bo}})q_b} \quad (4)$$

where η is the energy recovery efficiency, p_{bi} is brine inlet pressure, p_{bo} is brine outlet pressure, p_{si} is seawater inlet pressure, p_{so} is seawater outlet pressure, q_b is the flow rate of brine stream, q_s is the flow rate of seawater stream.

Due to the eliminable short circuit leakage by the matching design and the eliminable vane tip leakage by ensuring the contact performance between the cylinder and vane which will be discussed below, the research in this paper is based on neglecting the internal leakage relying on the smooth transition design of the cylinder wall and the precision machining of the device. Then, the brine and seawater streams have equal flow rates. The volumetric efficiency defined as the ratio of seawater stream flow rate to the brine stream flow rate equals 100% (Eq. (5)):

$$\eta_v = \frac{q_s}{q_b} = 100\% \quad (5)$$

where η_v is the volumetric efficiency of the SVPE.

The hydraulic efficiency is defined as the ratio of the increase of pressure in the seawater stream to the decrease of pressure in the brine stream:

$$\eta_h = \frac{p_{\mathrm{so}} - p_{\mathrm{si}}}{p_{\mathrm{bi}} - p_{\mathrm{bo}}} \quad (6)$$

where η_h is the hydraulic efficiency of the SVPE.

Therefore, the energy recovery efficiency η of the SVPE can be written by the product of the hydraulic efficiency and the volumetric efficiency:

$$\eta = \eta_h \eta_v \quad (7)$$

Friction resistance torques lead to power reduction of the SVPE. Fig. 6 shows the position of the resistance torques. The resistance torque in the vane tip, M_{vt}, locates in the contact point between the vane tip and cylinder wall. The resistance torques in the vane sides, M_{vs}, locate in the contact points between the vane sides and vane slot. The resistance torques M_{reu} and M_{rel}, caused by viscous drag, locate between rotor upper end face and upper end plate and between rotor lower end face and lower end plate, respectively. The resistance torque M_{rs}, caused by viscous drag, locates between rotor side face and cylinder wall.

The vane tip friction torque of a single vane caused by the friction between vane tip and cylinder wall is expressed as Eq. (8):

$$M_{vt}(\theta) = \mu_1 F_{nt} \cos\delta r(\theta) \tag{8}$$

where $M_{vt}(\theta)$ is vane tip friction torque, $r(\theta)$ is the radial coordinate of the cylinder profile.

The vane side friction torque of a single vane caused by the friction between vane side and vane slot is calculated by Eq. (9):

$$M_{vs}(\theta) = \frac{\mu_2}{\omega}\left|F_{n1}v_r(\theta) + F_{n2}v_r(\theta)\right| \tag{9}$$

where $M_{vs}(\theta)$ is vane side friction torque, $v_r(\theta)$ is the vane relative velocity against vane slot, ω is the angular velocity of the rotor and can be calculated by: $v_r(\theta) = \omega dr(\theta)/d\theta$.

Then, the total friction torque associated with all the vanes is:

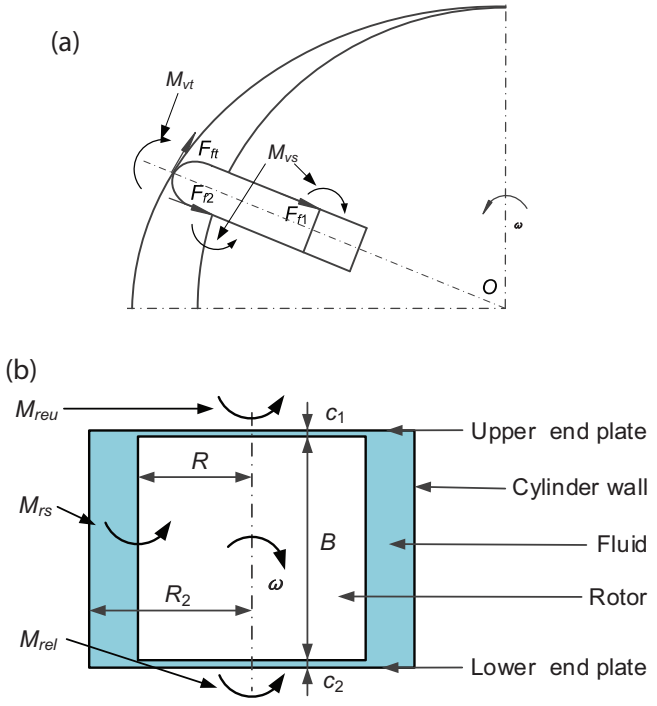

Fig. 6. Schematic diagram of position of the resistance torques. (a) Resistance torques generated by the vane and (b) resistance torques due to viscous drag.

$$M_v(\theta) = \sum_{k=1}^{z}[M_{vt}(\theta + (k-1)\gamma) + M_{vs}(\theta + (k-1)\gamma)] \tag{10}$$

where $M_v(\theta)$ is total vane friction torque, z is the number of the vane, k is the number counting for vanes and γ is the angle between neighboring two vanes.

The rotor end face resistance torque and rotor side face resistance torque are caused by the viscous drag of fluid which is assumed Couette flow, which can be obtained by Newton's law of viscosity equation:

$$M = \mu\frac{du}{dx}SL \tag{11}$$

where M is friction resistance torque, μ is fluid viscosity, du/dx is velocity gradient, S is rotor radial area and L is torque radius.

Based on Eq. (11), the rotor side face resistance torque can be calculated by Eq. (12). The mean clearance between the rotor side face and cylinder wall is considered to be the average value of the maximum clearance and the minimum clearance, Eq. (13):

$$M_{rs} = \frac{\mu n\pi^2}{15}\frac{R^3 B}{c_m} \tag{12}$$

$$c_m = \frac{R_2 - R}{2} \tag{13}$$

where n is the rotational speed of the rotor, R_2 is major radius of the cylinder, R is rotor radius which equals the minor radius of the cylinder R_1, B is the axial length of the rotor, c_m is the mean value of the clearance between the rotor side face and cylinder wall.

The resistance torque of the upper and lower rotor end faces are calculated by:

$$M_{reu} = \frac{\mu n\pi^2}{60c_1}R^4 \tag{14}$$

$$M_{rel} = \frac{\mu n\pi^2}{60c_2}R^4 \tag{15}$$

where M_{reu} and M_{rel} are upper and lower rotor end face resistance torques, respectively, c_1 and c_2 are upper and lower rotor end face clearance, respectively.

Then, the total rotor end face resistance torque is:

$$M_{re} = M_{reu} + M_{rel} \tag{16}$$

where M_{re} is rotor end face resistance torque.

Hence, the total friction power loss W_t including the friction loss generated by vanes and the friction loss due to the viscous drag can be expressed as:

$$W_t = \frac{\omega}{2\pi}\int_0^{2\pi} M_v(\theta)d\theta + \omega(M_{rs} + M_{re}) \tag{17}$$

The friction power loss is considered to be the energy loss in the energy recovery process, and the calculated value of the energy recovery efficiency can be expressed by:

$$\eta_{cal} = 1 - \frac{W_t}{(p_{bi} - p_{bo})q_b} \tag{18}$$

where η_{cal} is the calculated value of the energy recovery efficiency based on the energy loss.

2.4. Flowchart for determining energy recovery efficiency

The energy recovery efficiency is simulated based on the mass and energy conservation. The default parameter settings are shown in Table 2. The brine inlet pressure p_{bi}, brine outlet pressure p_{bo} and seawater inlet pressure p_{si} are given parameters that can be controlled by operators. The pressurized seawater stream is the target fluid, and its pressure p_{so} is an unknown parameter and determined by the energy recovery efficiency η. That is to say, the efficiency η and seawater outlet pressure p_{so} are the only correspondence. With the given structural parameters (including vane thickness t, vane length h, etc.) and operational parameters (including rotational speed n, brine inlet pressure p_{bi}, brine outlet pressure p_{bo}, seawater inlet pressure p_{si}), the efficiency η (or seawater outlet pressure p_{so}) is the only unknown parameter.

Fig. 7 shows the flowchart for determining the energy recovery efficiency of the SVPE. With an assumed value of the energy recovery efficiency η which corresponds to a seawater outlet pressure p_{so}, the calculation process is carried out. The vane dynamics model is used to evaluate the contact performance between the cylinder and vane. The device parameters are adjusted if the vane cannot always contact with the cylinder in the middle section. Under the premise of well contact performance, the energy loss model is utilized to calculate the energy loss in the energy recovery process. The calculated value of energy recovery efficiency η_{cal} is obtained according to Eq. (18), and then is used to update the assumed value of energy recovery efficiency until the convergence of the computational process is achieved.

Table 2
Default parameter settings

Parameter	Value
Rotor radius (R), mm	70
Minor radius of cylinder wall (R_1), mm	70
Major radius of cylinder wall (R_2), mm	85
Rotational speed (n), rpm	2,000
Vane thickness (t), mm	15
Vane length (h), mm	45
Vann tip friction coefficient (μ_1)	0.05
Vane side friction coefficient (μ_2)	0.05
Rotor axial length (B), mm	30
Upper rotor end face clearance (c_1), mm	0.02
Lower rotor end face clearance (c_2), mm	0.02
Vane material density (ρ), kg/m^3	3,700
Brine inlet pressure (p_{bi}), MPa	6.00
Brine outlet pressure (p_{bo}), MPa	0.03
Seawater inlet pressure (p_{si}), MPa	0.03

3. Results and discussion

3.1. Contact performance

The contact performance between the cylinder and vane has a vital impact on the energy recovery process of SVPE. The contact status is characterized by the value of the contact force F_{nt}. The vane should always contact with the cylinder in the middle section, which means that the positive value of contact force F_{nt} in the middle section should be ensured.

It can be found from the results that the contact status between the cylinder and vane obviously varies with rotational speed n, vane thickness t and vane length h. The critical parameters are used to define the critical contact performance that the vane can nicely always contact with the cylinder in the middle section. Figs. 8–10 show the critical rotational speed n_c, critical vane thickness t_c and critical vane length h_c varying with other parameters, respectively. It can be observed from Fig. 8 that the critical rotational speed decreases with the vane thickness and vane length, respectively. The critical vane thickness decreases with rotational speed and vane length, respectively (Fig. 9). As Fig. 10 shows the critical vane length decreases with rotational speed and vane thickness, respectively. Among the rotational speed, vane thickness and vane length, the critical value of one parameter decreases with the other two parameters, respectively. In other words, increasing rotational speed, vane thickness and vane length are all beneficial to the well contact performance. And the device can be reasonably designed to guarantee the well contact performance.

3.2. Comparison analysis

The simulated results of the efficiency in this work have been compared with those in the study by Al-Hawaj [14],

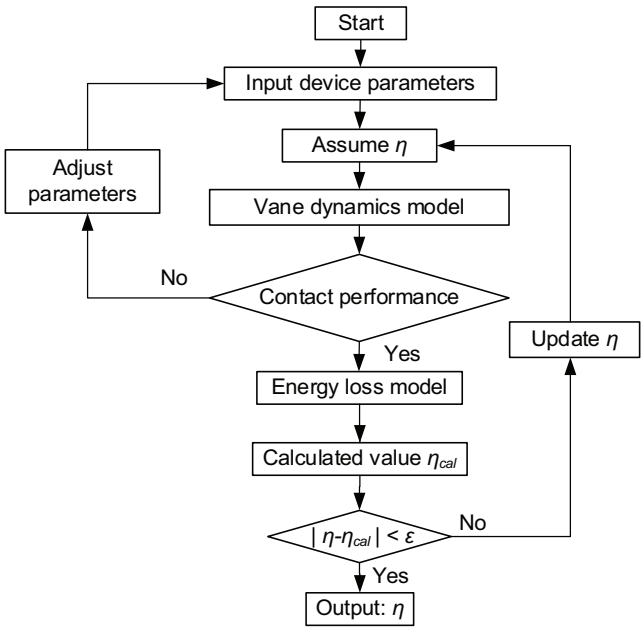

Fig. 7. Flowchart for determining energy recovery efficiency.

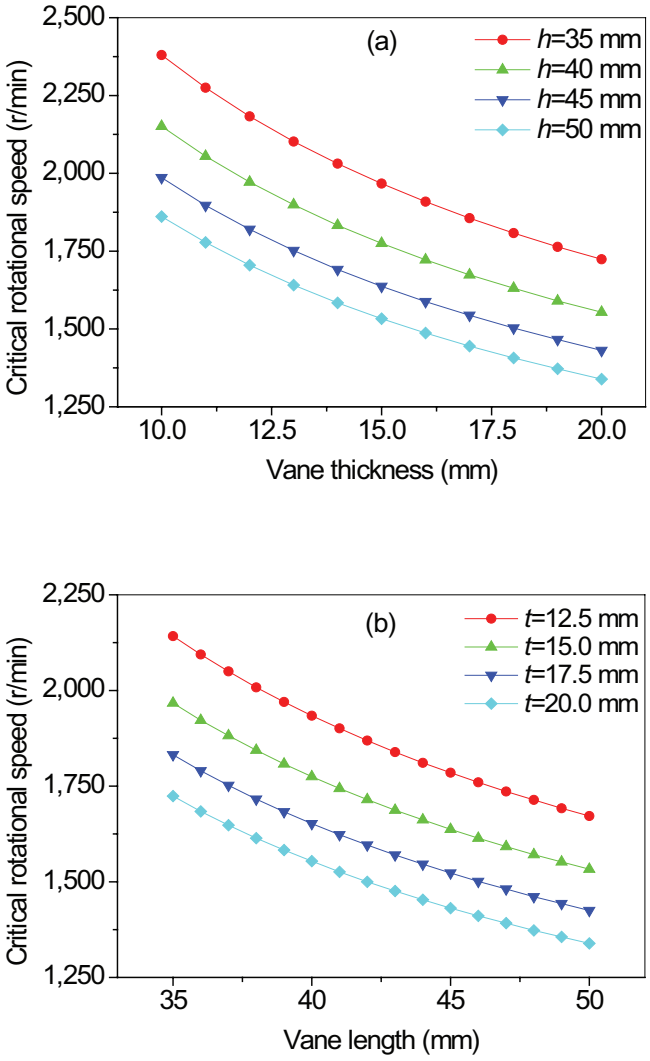

Fig. 8. Critical rotational speed varying with (a) vane thickness and (b) vane length.

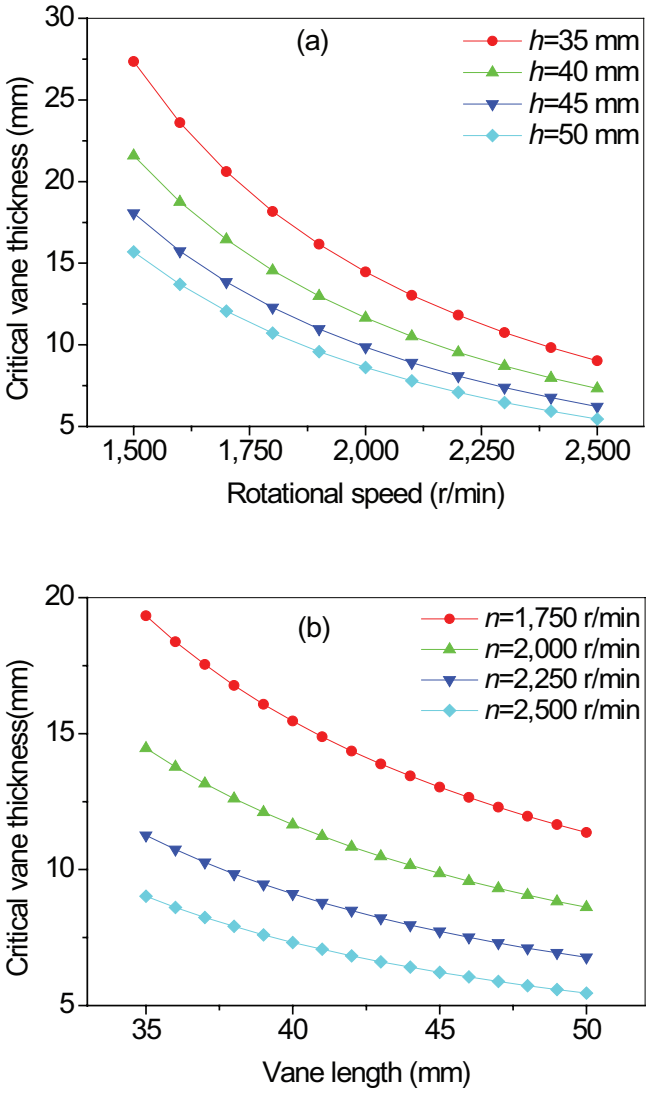

Fig. 9. Critical vane thickness varying with (a) rotational speed and (b) vane length.

as shown in Figs. 11 and 12. Considering the influences of rotational speed and vane thickness on the hydraulic efficiency η_h of the SVPE, the cures of simulated values in this work and the work by Al-Hawaj [14] follow a similar trend. This outcome makes an acceptable qualitative validation of the method for determining the energy recovery efficiency used in this paper. The vane tip leakage and short circuit leakage are used to determine the volumetric efficiency η_v of the SVPE in the study by Al-Hawaj [14]. In the simulation model of this work, the vane tip leakage and the short circuit leakage are considered to be eliminated by the well contact performance between the cylinder and vane in the middle section and the matching design of the vane number and port position, respectively, resulting in the ideal value 100% of the volumetric efficiency η_v. Therefore, the energy recovery efficiency η equals the hydraulic efficiency η_h in this work. The volumetric efficiency η_v in this work is higher than that in the reference, which contributes to the higher energy recovery efficiency η of the SVPE in this work.

3.3. *Efficiency discussion*

Under the premise of well contact performance, the influences of rotational speed, vane thickness and vane length on the energy recovery efficiency are studied by the developed method. Figs. 13–15 show the energy recovery efficiency varying with rotational speed, vane thickness and vane length, respectively. It can be observed from Fig. 13 that the energy recovery efficiency decreases with rotational speed. In each rotational cycle of the vane, the effect of increasing rotational speed results in increasing centrifugal forces on vanes, which leads to increasing contact force and friction loss in vane tip, and then decreasing the efficiency. According to Fig. 14, the energy recovery efficiency decreases with vane thickness. Larger vane thickness is associated with larger centrifugal forces due to the increase of vane mass. At the same time, increasing vane thickness leads to increasing vane base force due to increasing vane cross-sectional area. Both effects lead to increasing contact force and friction loss in vane tip.

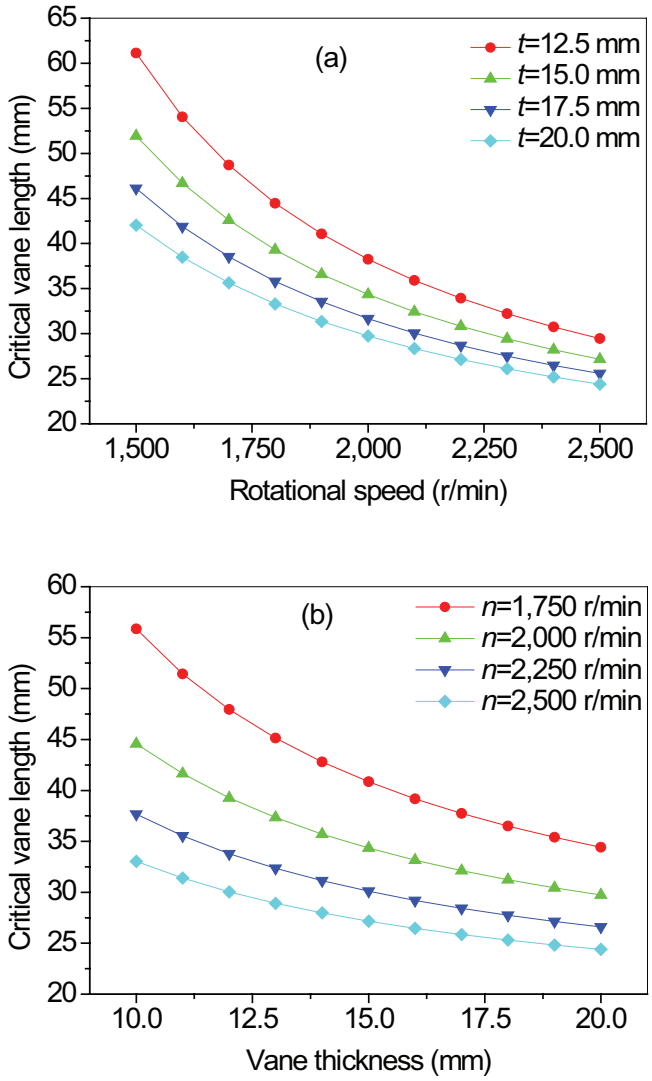

Fig. 10. Critical vane length varying with (a) rotational speed and (b) vane thickness.

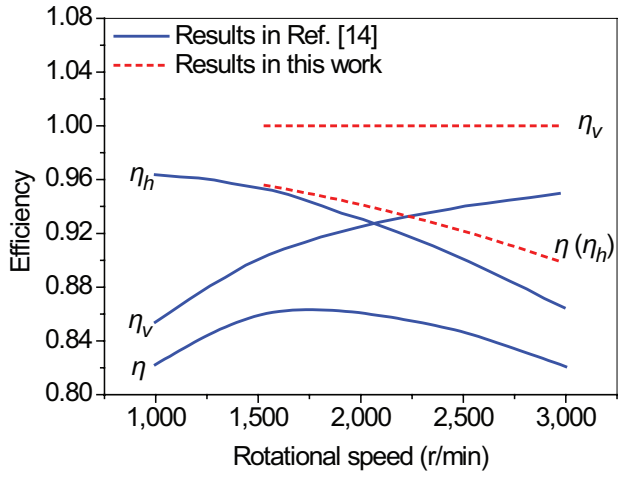

Fig. 11. Comparison of the effect of rotational speed on the efficiency of SVPE between the work by Al-Hawaj [14] and this work.

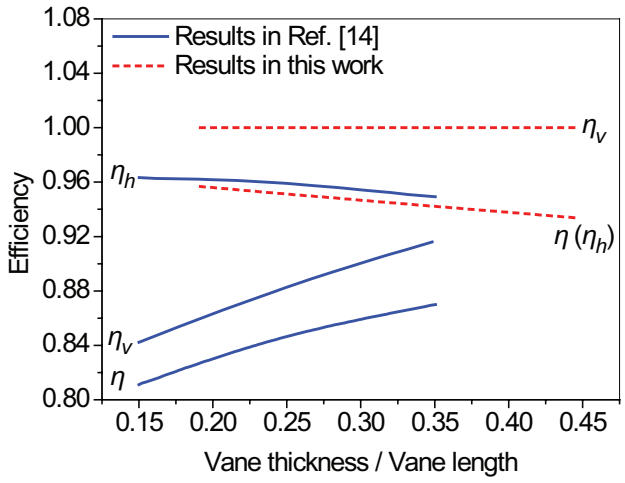

Fig. 12. Comparison of the effect of vane thickness on the efficiency of SVPE between the work by Al-Hawaj [14] and this work.

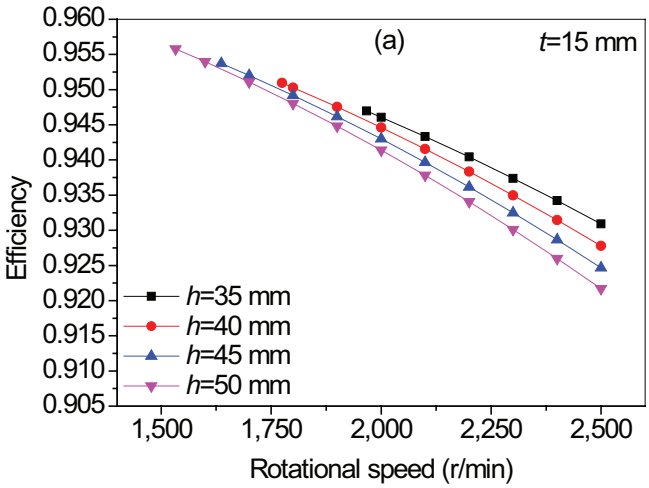

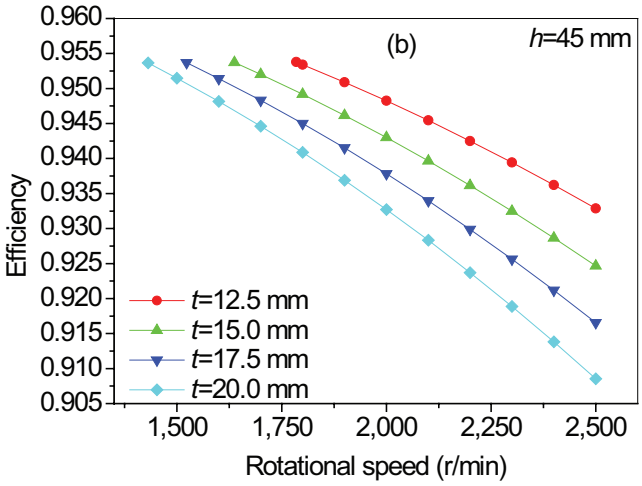

Fig. 13. Effect of rotational speed on energy recovery efficiency with (a) a constant vane thickness of 15 mm and (b) a constant vane length of 45 mm.

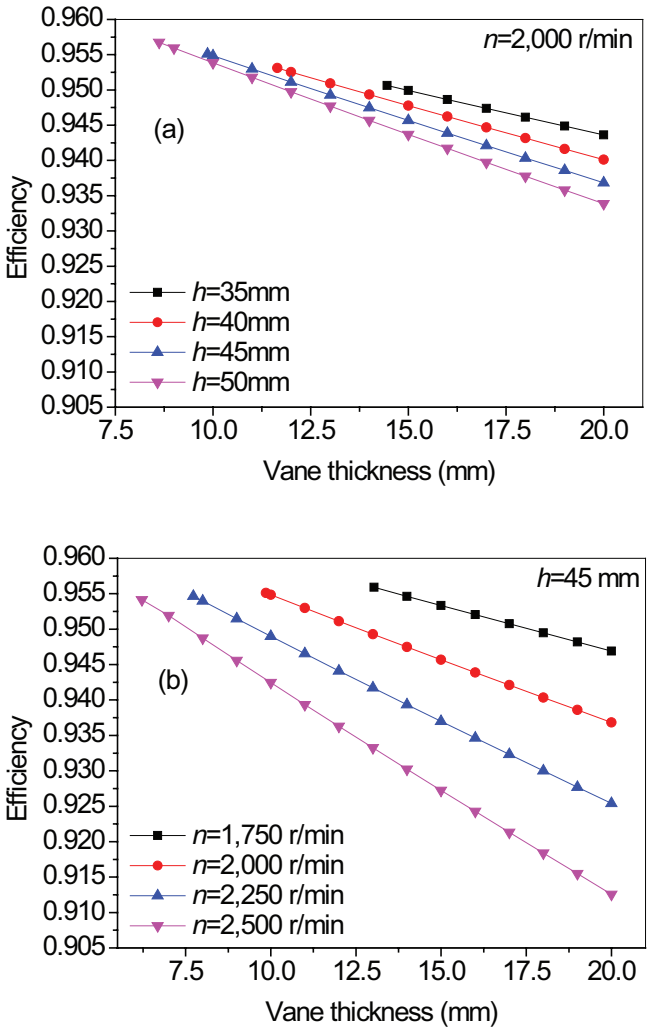

Fig. 14. Effect of vane thickness on energy recovery efficiency with (a) a constant rotational speed of 2,000 rpm and (b) a constant vane length of 45 mm.

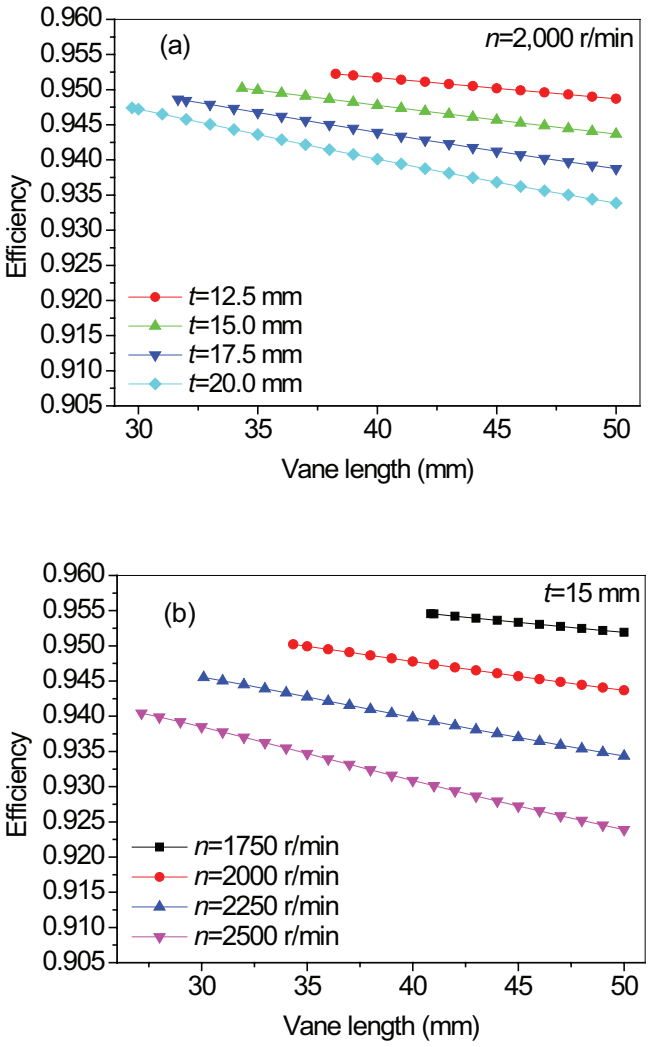

Fig. 15. Effect of vane length on energy recovery efficiency with (a) a constant rotational speed of 2,000 rpm and (b) a constant vane thickness of 15 mm.

As shown in Fig. 15, the energy recovery efficiency slightly decreases with vane length as a whole. Increasing vane length results in larger centrifugal forces due to increasing vane mass, leading to more vane tip friction loss. But meanwhile, the vane center is closer to the rotor center, which improves the force status of the vane. The two opposite effects result in a slight decline in the efficiency. In general, increasing rotational speed, vane thickness and vane length have negative effects on the energy recovery efficiency.

Regarding Fig. 13(a), with a constant vane thickness of 15 mm, when the vane length is 35, 40, 45 and 50 mm, the maximum efficiency is 0.947, 0.951, 0.954 and 0.956, respectively. And the rotational speeds associated with the maximum efficiency are all critical rotational speeds. It means that the maximum efficiency increases with vane length when vane thickness is constant. Similarly, the maximum efficiency decreases with vane thickness when vane length is constant, as shown in Fig. 13(b). The maximum efficiency increases with vane length when rotational speed is constant (Fig. 14(a)) and decreases with rotational speed when vane length is constant (Fig. 14(b)). As shown in Figs. 15(a) and (b), the maximum efficiency decreases with vane thickness when rotational speed is constant and decreases with rotational speed when vane thickness is constant, respectively. And the corresponding parameters associated with the maximum efficiency are all critical parameters. According to Figs. 13–15, the energy recovery efficiency of SVPE ranges from 90.9% to 95.7% under different rotational speed, vane thickness and vane length. By calculation, the maximum efficiency can achieve 95.7% when the rotational speed, the vane thickness and the vane length are 2,000 rpm, 8.62 mm and 50 mm, respectively, and it obviously exceeds the efficiency of the centrifugal type ERDs and approximates the efficiency of the positive displacement type ERDs.

4. Conclusions

In this work, a method is developed to accurately evaluate the energy recovery efficiency of a SVPE based on the mass and energy conservation. The three-vane SVPE

matched with the port edge angles are designed and used to carry out following analysis. The similar trend of the simulated results between in this work and in the reference qualitatively verifies the accuracy of the method for evaluating the efficiency of SVPE in this work. Decreasing rotational speed, vane thickness and vane length are all beneficial to achieve higher energy recovery efficiency, but not conducive to the well contact performance between the cylinder and vane. The energy recovery efficiency of SVPE ranges from 90.9% to 95.7% under different device parameters, and the maximum efficiency can achieve 95.7% by calculation which approximates the efficiency of the positive displacement type ERDs. The results suggest that the SVPE is of reasonable structure, convenient manufacture and high efficiency, and present considerable potential of the SVPE to be an efficient pressure ERD for SWRO system.

Acknowledgment

It is acknowledged that this paper has been supported by the National Natural Science Foundation of China (Grant No. 21376187).

References

[1] M. Elimelech, W.A. Phillip, The future of seawater desalination: energy, technology, and the environment, Science, 333 (2011) 712–717.
[2] S. Kumarasamy, S. Narasimhan, S. Narasimhan, Optimal operation of battery-less solar powered reverse osmosis plant for desalination, Desalination, 375 (2015) 89–99.
[3] J.M. Lee, H.W. Lee, Y.J. Kim, H.G. Park, S.P. Hong, J.Y. Koo, Improving fouling resistance of seawater desalination membranes via surface modification, J. Water Reuse Desal., 3 (2013) 217–223.
[4] B. Qi, Y. Wang, S. Xu, Z. Wang, S. Wang, Operating energy consumption analysis of RO desalting system: effect of membrane process and energy recovery device (ERD) performance variables, Ind. Eng. Chem. Res., 51 (2012) 14135–14144.
[5] A. Altaee, G.J. Millar, G. Zaragoza, A. Sharif, Energy efficiency of RO and FO–RO system for high-salinity seawater treatment, Clean Technol. Environ., 19 (2016) 77–91.
[6] R.L. Stover, Development of a fourth generation energy recovery device. A 'CTO's notebook', Desalination, 165 (2004) 313–321.
[7] R. Lemes, R. Falcon, R. Arocha, J. Curbelo, V. Platas, L.D. Lorenzo, Different designs in energy savings of SWRO Plant of Las Palmas III, Desal. Wat. Treat., 51 (2013) 749–758.
[8] R. Stover, J. Martin, Titan PX-1200 energy recovery device — test results from the Inima Los Cabos, Mexico, seawater RO facility, Desal. Wat. Treat., 3 (2009) 179–182.
[9] A. Zhu, P.D. Christofides, Y. Cohen, Effect of thermodynamic restriction on energy cost optimization of RO membrane water desalination, Ind. Eng. Chem. Res., 48 (2009) 6010–6021.
[10] R.L. Stover, Retrofits to improve desalination plants, Desal. Wat. Treat., 13 (2010) 33–41.
[11] Z. Cao, J. Deng, W. Yuan, Z. Chen, Integration of CFD and RTD analysis in flow pattern and mixing behavior of rotary pressure exchanger with extended angle, Desal. Wat. Treat., 57 (2016) 15265–15275.
[12] Y. Wang, Y. Ren, J. Zhou, E. Xu, S. Xu, Functionality test of an innovative single-cylinder energy recovery device for SWRO desalination system, Desalination, 388 (2016) 22–28.
[13] I.B. Cameron, R.B. Clemente, SWRO with ERI's PX Pressure Exchanger device — a global survey, Desalination, 221 (2008) 136–142.
[14] O.M. Al-Hawaj, Theoretical analysis of sliding vane energy recovery device, Desal. Wat. Treat., 36 (2011) 354–362.
[15] H.J. Kin, Numerical study on the performance improvement of a rotary vane expander for a CO_2 heat pump cycle, Int. J. Air-Cond. Refrig., 19 (2011) 311–319.